CMS Physics Analysis Summary

Search for new physics in events with two low momentum opposite-sign leptons and missing transverse energy at $\sqrt{s} = 13$ TeV

The CMS Collaboration

Abstract

A search for new physics in events with low-momentum opposite-sign leptons and missing transverse momentum, using 35.9 fb^{-1} of integrated luminosity collected by CMS experiment at $\sqrt{s} = 13$ TeV, is presented. The data observed are consistent with expectations from the standard model. The results are interpreted in terms of pair production of charginos and neutralinos ($\tilde{\chi}_1^{\pm}$, $\tilde{\chi}_2^0$) with nearly degenerate masses, as expected in natural compressed higgsino models, and in terms of the pair production of top squarks for the case that the neutralino and the top squark have similar masses. At 95% confidence level, $\tilde{\chi}_1^{\pm}/\tilde{\chi}_2^0$ are excluded for masses up to 230 GeV for a mass difference of 20 GeV with respect to the lightest neutralino, which is a region constrained so far by the LEP experiments only. An interpretation is also provided in terms of top squark ($\tilde{t}$) pair production processes with degenerate mass spectra and chargino-mediated decays. Masses of the $\tilde{t}$ up to 450 GeV are excluded for a mass difference of 40 GeV with respect to the lightest neutralino.

1 Introduction

Supersymmetry (SUSY) [1–5] is one of the most appealing extensions of the standard model (SM) of particle physics, as it can provide solutions to several pending questions in the SM, in particular those related to the mass hierarchy of elementary particles [6, 7]. SUSY predicts superpartners of SM particles (sparticles) whose spins differ by one-half unit with respect to their SM partners. In SUSY models with R-parity [8] conservation, sparticles are pair-produced and their decay chains end with the lightest supersymmetric particle (LSP), which in many models is the lightest neutralino ($\tilde{\chi}_1^0$). The latter, as a neutral and weakly interacting particle, matches the characteristics required of a dark matter candidate. In R-parity conservation, the LSPs would remain undetected in the detector and yield a characteristic signature of high missing transverse energy in the event (E_T^{miss}).

Following the first years of data-taking at the LHC, significant constraints have been placed on SUSY models, typically resulting in lower mass limits for various SUSY particles. Nevertheless, there are scenarios in which SUSY particles with lower masses could have escaped detection by existing searches. In particular, when the mass splitting between the next-to-lightest SUSY particle and the LSP is small, a scenario referred to as "compressed mass spectrum", the visible energy in the event, and by inference the E_T^{miss} as well, are relatively low. As a result, the mainstream searches, which are based on the presence of large E_T^{miss} and energetic final-state objects such as leptons and hadronic jets, are less sensitive to compressed mass spectrum scenarios.

Compressed mass spectra scenarios can arise in several SUSY models, including in natural SUSY: it has been pointed out by several authors, for example Refs. [6, 7, 9–14], that naturalness imposes constraints on the masses of higgsinos, top squarks and gluinos. Natural SUSY is generally considered with requiring at least one coloured particle to have relatively low mass, below ~ 1 TeV. It is further commonly assumed that this particle would be a third-generation squark, e.g. the top squark. More recently, however, the hypothesis of a light top squark has been disputed as arising from an oversimplified calculation [15]. Irrespective of the top squark, higgsinos remain a complementary window to natural SUSY since they are generally expected to be light. As pointed out in Refs. [15–17], light higgsinos would likely have a compressed mass spectrum, potentially leading to signatures with soft leptons and moderate or significant E_T^{miss}. Thus far, the most sensitive searches in this scenario have been carried out by experiments at LEP [18, 19].

The search described in this note has been conceived to search for signs of gauginos, which are also referred to as "electroweakinos", in a scenario where the latter form a compressed mass spectrum [16, 17, 20]. The search has discovery potential also for the case that a light top squark and the LSP are nearly degenerate in mass and the top squark decays to four fermions. A more detailed discussion of such a scenario can be found in Ref. [21]. The near-degeneracy in mass of the top squark and the LSP is typical of the so-called "co-annihilation region", which allows for dark matter to be provided solely by the LSP of SUSY [22].

In these scenarios, the visible decay products in the SUSY signal have low momentum and the signal events can be distinguished from SM processes if a high transverse momentum jet from initial-state radiation (ISR) leads to a boost of the sparticle pair system and enhances the E_T^{miss} in the event, while the other decay products typically remain soft. The search strategy based on the presence of an ISR jet has been used to search for the two-body decay in a monojet topology by the CMS Collaboration [23], and for both decay modes by the ATLAS Collaboration [24, 25]. In the signal scenarios studied in this note, SUSY particles can decay leptonically, and the presence of low transverse momentum (p_T) leptons can be used to discriminate further against otherwise dominant SM backgrounds, such as multijet production and Z+jets events

with invisible Z boson decays.

The strategy of the current analysis, for data corresponding to 35.9 fb^{-1} of luminosity at 13 TeV, is similar to the previous publication for the 8 TeV data [26]. The main difference lies in the deployment of a new trigger selection, which improves the sensitivity of the search. The selection in [26] has also been extended to be optimal for electroweakinos in a compressed mass spectrum. As in the 8 TeV analysis, events containing a b-tagged jet are rejected, in order to reduce the significant background from $t\bar{t}$ production. At least one jet is required in the final state which, in the case of the signal, must arise from ISR which provides the final-state particles with a boost in the transverse plane and thus the potential for a moderate or large missing transverse energy in the event. Contrary to the 8 TeV analysis, the search is inclusive in the number of jets, i.e. there is no upper limit on the number of jets in the event.

2 CMS detector

The central feature of the CMS apparatus is a superconducting solenoid of 6 m internal diameter, providing a magnetic field of 3.8 T. Within the superconducting solenoid volume a silicon pixel and strip tracker, a lead tungstate crystal electromagnetic calorimeter (ECAL), and a brass and scintillator hadron calorimeter (HCAL), each composed of a barrel and two endcap sections, are located in concentric layers. These layers provide coverage out to a pseudorapidity $|\eta| = 2.5$. Together with the magnet, the tracking system allows for tracks with transverse momentum p_T as low as 100 MeV to be reconstructed, and give a p_T resolution of 1% at 100 GeV. The ECAL electromagnetic transverse energy resolution is of about $3\%/\sqrt{E_T/\text{GeV}}$, and the HCAL transverse hadronic energy resolution is of about $100\%/\sqrt{E_T/\text{GeV}}$. Muons are measured in gas-ionization detectors embedded in the steel flux-return yoke outside the solenoid. A forward calorimetry complements are provided by the barrel and endcap detectors up to $|\eta| < 5.2$. The first level (L1) of the CMS trigger system uses information from the calorimeters and muon detectors to select the most interesting events in a fixed time interval of less than 4 μs. The high-level trigger (HLT) processor farm further decreases the event rate from around 100 kHz to around 400 Hz before data storage. A more detailed description of the CMS detector, together with a definition of the coordinate system used and the relevant kinematic variables, can be found in Ref. [27].

3 Data and simulated samples

The data used in this search correspond to 35.9 fb^{-1} of pp collisions at a centre-of-mass energy of 13 TeV, recorded in 2016 with the CMS detector. The data are selected with two triggers: an inclusive E_T^{miss} trigger, with a threshold that varied from an initial value of 90 GeV to larger values as the instantaneous luminosity of the LHC increased. The second trigger was introduced after the first technical stop of the LHC in 2016, with the requirement of two muons with $p_T > 3$ GeV and a lower threshold on E_T^{miss} of 50 GeV. The sample with inclusive E_T^{miss} triggers corresponds to an integrated luminosity of 35.9 fb^{-1}, whereas the sample recorded with the dimuon + E_T^{miss} trigger corresponds to 33.2 fb^{-1}.

Simulated samples of the signal, $t\bar{t}$, W+jets, and Z+jets processes are generated at leading-order (LO) with the MADGRAPH5 [28] event generator, using the NNPDF3.0LO [29] parton distribution functions (PDFs). For di-bosons, single top quark and rare processes, the next-to-leading order generators MADGRAPH5_aMC@NLO [30] and POWHEGv1.0 [31–35] are used with the NNPDF3.0NLO [29] PDFs. Showering and hadronization is carried out by the PYTHIA 8.2

package [36], while a detailed simulation of the CMS detector is based on the GEANT4 [37] package. A fast detector simulation [38] is used for large samples of signal corresponding to different sparticle masses, the so-called "signal scans".

We consider a mass scan for neutralino-chargino ($\tilde{\chi}_2^0$-$\tilde{\chi}_1^\pm$) pair production where the $\tilde{\chi}_2^0$ and $\tilde{\chi}_1^\pm$ are assumed to decay to the LSP via virtual Z^* and W^* bosons. For the virtual Z^* boson, the SM branching fractions for decays to the different fermions are assumed. These branching fractions are a function of the maximal fermion pair mass $M(ff)$, which is the mass difference between $\tilde{\chi}_2^0$ and $\tilde{\chi}_1^0$. The simulation of the $\tilde{\chi}_2^0$ decay takes the Breit-Wigner of the Z boson into account. The production cross sections used correspond to those for pure Wino production [39, 40]. The second scan simulates a simplified model of $\tilde{t}$-pair production, in which the chargino mediates the decay of the $\tilde{t}$ into leptons and $\tilde{\chi}_1^0$, namely $\tilde{t} \to \tilde{\chi}_1^\pm b$ followed by $\tilde{\chi}_1^\pm \to \tilde{\chi}_1^0 W^*$. The mass of the $\tilde{\chi}_1^\pm$ is set to $(M_{\tilde{t}} + M_{\tilde{\chi}_1^0})/2$ and the mass difference between $\tilde{t}$ and $\tilde{\chi}_1^0$ is set to be less than 90 GeV. Figure 1 illustrates the signal models considered.
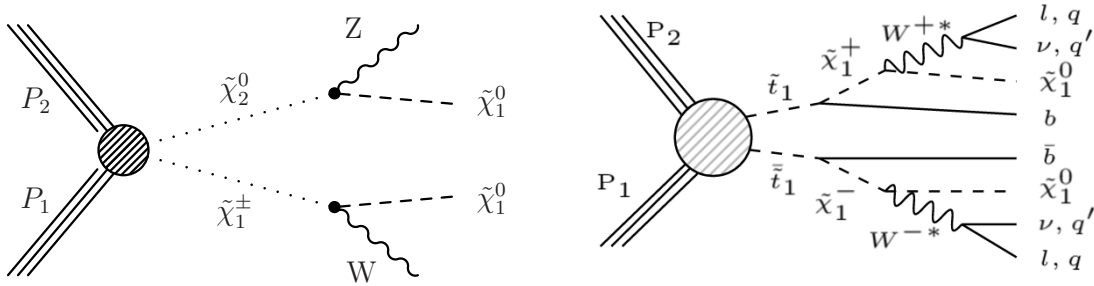

Figure 1: Left: electroweakino pair production and decay. Right: chargino-mediated $\tilde{t}$ pair production and decay.

4 Object reconstruction

The physics objects used in the analysis are reconstructed and selected using CMS particle flow (PF) algorithms [41] and requirements. The PF algorithm reconstructs individual particles by combining information from all sub-detector systems. The difficulties in reconstructing the event of interest, due to the average number of interactions per bunch crossing (pileup), are mitigated using a primary vertex selection and other methods described below.

Primary vertices are identified using tracks clustered with the deterministic annealing algorithm [42]. The reconstructed primary vertex is chosen as the vertex with the largest quadratic sum of the p_T of its constituent tracks. Additionally, this vertex needs to be within 24 cm from the center of the detector in the z direction and within 2 cm on the plane transverse to the beam line.

Leptons are required to have p_T and η inside the trigger acceptance and within the boundaries of the inner tracker. The leading muon (electron) is thus required to satisfy $p_T > 5\,\text{GeV}$, $|\eta| <$ 2.4 ($|\eta| < 2.5$). An upper requirement of $p_T < 30\,\text{GeV}$ on the leading lepton is also applied; this threshold is identified as the p_T value below which the current analysis is more sensitive in excluding the benchmarks in the compressed regions, compared to other analyses in CMS. In order to further increase the sensitivity to the compressed regime, in some parts of the analysis the lower threshold on the p_T of the subleading muon is set to 3.5 GeV.

Muons are required to pass soft muon identification criteria [43] and to be isolated within a cone in $\eta - \phi$ space of radius $\Delta R = \sqrt{\Delta\eta^2 + \Delta\phi^2} < 0.3$: the sum of the transverse momenta

within the cone, Iso_{abs}, are required to be less than 5 GeV. In addition, the quantity Iso_{rel}, which is the ratio of Iso_{abs} and the p_{T} of the muon, is required to be less than 0.5. Contamination from pileup within the isolation cone is subtracted using techniques that utilise charged deposits inside the cone itself [43].

Identification of electrons from prompt decays is performed using a multivariate discriminant based on shower shape and track quality variables. The loose working point (WP) employed by the $H \to ZZ^* \to 4\ell$ analysis [44] is used for $p_{\mathrm{T}} < 10$ GeV, and a tighter one for $p_{\mathrm{T}} > 10$ GeV. The same isolation criteria as for muons are applied. To suppress non-prompt leptons, requirements on the impact parameter with respect to the primary vertex, in three dimensions, IP_{3D}, and its significance, SIP_{3D}, are applied: leptons are required to have $IP_{3D} < 0.01$ cm and $SIP_{3D} < 2$.

Jets are clustered from the particles reconstructed by the PF algorithm [41]. In the jet clustering procedure, charged PF particles not associated with the primary vertex are excluded. The anti-k_{T} jet clustering algorithm [45] is used with a distance parameter R = 0.4. The jet energy scale (JES) is measured in data using dijet and photon plus jets events, and a correction to the energy of the jet is applied to both data and simulated samples. Jets are selected with $p_{\mathrm{T}} > 25$ GeV and $|\eta| < 2.4$. In the following, the transverse hadronic energy, H_{T}, is defined as the scalar sum of the transverse momenta of the selected jets.

Jets arising from the hadronization of b quarks are identified with the Combined Secondary Vertex (CSVv2) tagger [46]. In this analysis a loose working point (CSVv2L), which has a nominal efficiency of about 80% (for a udsg-mistag efficiency of 10%) is used. Since the analysis focuses on final states with soft leptons, b-jets events tagged by this tagger with $p_{\mathrm{T}} > 25$ GeV are vetoed. This allows potential soft b-tagged jets in e.g. the compressed $\tilde{\mathrm{t}}$-LSP scenario.

The magnitude of the missing transverse momentum, i.e. the momentum imbalance in the event, $E_{\mathrm{T}}^{\mathrm{miss}}$, is determined using the PF reconstructed quantities. Various event filters are applied to remove detector- and beam-related noise.

5 Event selection

The analysis requires two opposite-sign (OS) leptons ($N_\ell = 2$), of either the same flavor (ee, $\mu\mu$) or different flavor ($e\mu$), and moderate missing transverse momentum in the final state, together with the presence of at least one jet in the event. Leptons and the hadronic content of the event, jets and $E_{\mathrm{T}}^{\mathrm{miss}}$, are identified according to the criteria listed in Section 4.

The complete set of requirements that define the search region (SR) is listed in Table 1. The main backgrounds arise from events in which one of the leptons is not prompt (mainly in W+jets events), events from fully leptonic $t\bar{t}$ decays, and Drell-Yan (DY) processes with subsequent decays $\gamma/Z^* \to \tau\tau \to \ell\ell\nu_\ell\nu_\ell\nu_\tau\nu_\tau$. Smaller backgrounds are relatively rare diboson processes like WW (VV) and t+W (tW) production. The event selection in Table 1 includes a number of requirements that are designed to reduce these backgrounds:

- $0.6< E_{\mathrm{T}}^{\mathrm{miss}}/H_{\mathrm{T}} <1.4$: this criterion is effective in rejecting QCD events while it is efficient for events with ISR, as in the case of the signal. The upper bound on the ratio $E_{\mathrm{T}}^{\mathrm{miss}}/H_{\mathrm{T}}$ is determined from a study of a control region at low $E_{\mathrm{T}}^{\mathrm{miss}}$ and dimuon mass around the J/ψ mass. This requirement rejects such events while leaving the signal unaffected.

- b-jet event veto: requiring events where no jet is tagged as originating from a b quark reduces significantly the $t\bar{t}$ background where the b jets are coming from the decay

of the top quarks. The requirement is applied to all jets with $p_T > 25$ GeV and using b-tag selection criteria described in Section 4.

- $M_{\tau\tau} < 0$ or $M_{\tau\tau} > 160$ GeV: this requirement is designed to reject the large background from $Z \to \tau\tau$ events, with the τ leptons subsequently decaying leptonically. The quantity $M_{\tau\tau}$ is computed as follows: since the τ leptons from Z boson decays have high momenta compared to their mass (m_τ), $p_T(\tau) \gg m_\tau$, the direction of the final lepton, i.e. the observed electron or muon, is approximately the same as that of the parent τ lepton (i.e. $\Delta R(\ell, \tau) \sim 0$). The magnitudes of the lepton vectors are then scaled so that the lepton pair balances the hadronic recoil. For $Z \to \tau\tau$ events, this leads to a fairly good approximation of the original τ momenta. The invariant mass of the two τ leptons, $M_{\tau\tau}$, is estimated as the invariant mass of the two scaled leptons. In some events, the estimate of the τ momentum magnitude takes a negative value when the flight direction is opposite to the lepton one. In these cases the invariant mass $M_{\tau\tau}$ is set to be negative.

- $M_T(\ell_i, E_T^{\text{miss}}) < 70$ GeV, i=1,2: for the signal, the leading lepton is typically aligned with the boost direction of the LSP ($\Delta\phi(l, E_T^{\text{miss}}) \sim 0$). This cut is effective in further suppressing the $t\bar{t}$ background for the electroweakino search, but not for the $\widetilde{t}$ search.

- J/ψ and Y veto: to suppress potential background contributions from J/ψ, γ^* and Y decays, the di-lepton invariant mass, $M(\ell\ell)$, is required to satisfy $M(\ell\ell) > 4$ GeV and also to lie outside the range $9 < M(\ell\ell) < 10.5$ GeV.

- $E_T^{\text{miss}} > 125$ GeV: to ensure high trigger efficiency for the kinematic region used in the analysis, both the E_T^{miss} and the muon-corrected $E_T^{\text{miss}}{}_{\text{corr}}$, which is computed from the vectorial sum of the E_T^{miss} and the p_T of the muons selected in the events, are required to be larger than 125 GeV.

- Trigger acceptance: at the trigger level the lepton pair is required to have a small boost of $p_T > 3$ GeV together with an upper bound on the dimuon invariant mass, $M(\ell\ell) < 60$ GeV, in order to limit the trigger rate. This imposes an upper cut of 50 GeV on the invariant mass of the leptons selected offline and a lower cut on the dilepton transverse momentum $p_T(\ell\ell) > 3$ GeV.

- $H_T > 100$ GeV: this requirement suppresses backgrounds with low hadronic activity in the event.

For the selected events above, a set of search regions (SRs) are defined, based on dilepton invariant mass and E_T^{miss}. For events with same-flavor and opposite-sign leptons, four SRs are defined in $M(\ell\ell)$ ranges of 4-10, 10-20, 20-30, and 30-50 GeV. These SRs are for events $\widetilde{\chi}_2^0 \to Z * \widetilde{\chi}_1^0$, where $M(\ell\ell)$ is inferring the mass difference between the two gauginos.

For events with different-flavor and opposite-sign leptons, three SRs are defined in the leading lepton p_T ranges 5-12, 12-20, 20-30, and 30-50 GeV. The threshold of the trailing lepton is reduced to 3.5 GeV for muons in the high E_T^{miss} region to gain sensitivity in the search for $\widetilde{t}$ signal.

To fully exploit the potential of the dimuon plus E_T^{miss} trigger introduced in 2016, events are separated according to the value of E_T^{miss}: in total three regions are used for the signal extractions, namely $E_T^{\text{miss}} = [125,200]$, $[200-300]$ and >300 GeV for the $\widetilde{t}$ search and $E_T^{\text{miss}} = [125,200]$, $[200-250]$ and >250 GeV for the electroweakino search. Since the low E_T^{miss} region contains events accessible only via the new trigger, only $\mu^+\mu^-$ pairs are considered. Conversely, in the high E_T^{miss} region both electron and muon flavors are considered. The electroweakino SRs are populated by e^+e^- and $\mu^+\mu^-$ pairs, while for the $\widetilde{t}$ SRs $e\mu$ pairs are also allowed.

Table 1: Selection requirements for the signal regions. The subleading lepton p_T threshold is reduced to 3.5 GeV for muons in the high E_T^miss $\widetilde{\text{t}}$-like signal region. Iso_rel and Iso_abs are relative and absolute isolation variables.

Variable	SR selection criteria
N_ℓ	$= 2$ (ee,$\mu\mu$, $e\mu$)
$Q(\ell_1)Q(\ell_2)$	-1
$p_\text{T}(\ell_1)$, $p_\text{T}(\ell_2)$	$[5, 30]$ GeV
$p_\text{T}(\mu_2)$ for high E_T^miss $\widetilde{\text{t}}$-like SR	$[3.5, 30]$ GeV
$|\eta_\mu|$	< 2.4
$|\eta_\text{e}|$	< 2.5
IP_{3D}	< 0.01 cm
SIP_{3D}	< 2
$Iso_\text{rel}(\ell_{1,2})$ & $Iso_\text{abs}(\ell_{1,2})$	< 0.5 && < 5 GeV
$p_\text{T}(jet1)$	> 25 GeV
$|\eta|(jet1)$	< 2.4
N_b (>25 GeV, CSVv2L)	$= 0$
$M(\ell\ell)$	< 50 GeV
$p_\text{T}(\ell\ell)$	> 3 GeV
E_T^miss	> 125 GeV
E_T^miss (muon subtracted)	> 125 GeV
$E_\text{T}^\text{miss} / H_\text{T}$	$[0.6, 1.4]$
H_T	> 100 GeV
$M(\ell\ell)$	> 4 GeV
$M(\ell\ell)$	veto$[9, 10.5]$ GeV
$M_{\tau\tau}$	veto$[0, 160]$ GeV
$M_\text{T}(\ell_x, E_\text{T}^\text{miss}), x = 1, 2$	< 70 GeV (for electroweakino selection only)

6 Background estimation

Backgrounds with two prompt leptons are estimated using control regions that are chosen to be similar in phase space to the signal regions, and yet remain relatively signal free. Different control regions are employed for each physics process that contributes significantly in the signal region, i.e. the $t\bar{t}$ dilepton background, the DY+jets background and the diboson background.

The background in the search regions is estimated for individual physics processes, using the number of events observed in the data in the corresponding control region (CR) and a transfer factor which describes the expected ratio of events in the SR and in the CR for each physics process. The transfer factor for a specific physics process, F_{process}, is determined from Monte Carlo (MC) simulation of the process as the ratio

$$F_{\text{process}} = \frac{N^{SR}_{\text{MC process}}}{N^{CR}_{\text{MC process}}}.$$

If the corresponding CR in the data consisted solely of events from the physics process in question, e.g. DY+jets events, then the expected background yields in the SR would be given as

$$N^{SR}_{\text{process}} = N^{CR}_{\text{data}} F_{\text{process}}.$$

This estimate assumes that the simulation describes well the kinematic dependence of the physics process, and normalizes the expected yield from the physics process in question to the one observed in the corresponding CR in the data. Deviations from this assumption are accounted for as systematic uncertainties in the value of the transfer factor.

In practice, each CR contains contributions from other physics processes that need to be subtracted from N^{CR}_{data}. These contributions, $N^{SR}_{\text{MC other}}$, are small compared to the main process for which the CR is defined, and are thus estimated using MC simulation. The final estimate of the background from a specific physics process in the SR is given by

$$N^{SR}_{\text{process}} = \left(N^{CR}_{\text{data}} - N^{SR}_{\text{MC other}} \right) F_{\text{process}}.$$

Systematic uncertainties on the value of F_{process} are included while determining the full uncertainty on N^{SR}_{process}. The total background in the SR is given as the sum of the backgrounds expected from each process in this method.

The different CRs are binned in $E^{\text{miss}}_{\text{T}}$, but not in $M(\ell\ell)$ or lepton p_{T}. A summary of all the CRs for prompt leptons is given in Table 2. For the diboson background, a validation region enriched in WW is added. This region is used to establish how well the simulation agrees with data in order to validate the uncertainty assigned to the diboson (VV) simulation.

Table 2: Summary of selection of control regions and the WW validation region (VR).

CR DY	CR tt(2l)	VR WW
no upper cut on p_{T} (ℓ) Relative isolation < 0.1 as OR to SR isolation		
$0 < \text{M}(\tau\tau)$ GeV < 160 $IP_{3D} < 0.0175$ cm, $SIP_{3D} < 2.5$		
p_{T} $(\ell 1) > 20$ GeV OR $IP_{3D} > 0.01$ cm OR $SIP_{3D} > 2$		p_{T} $(\ell 1) > 20$ GeV |SF $M(\ell\ell)$ - $M(Z)$ > 10 GeV
M_{T} as for EWKino SR	M_{T} as for stop SR	$\text{M}_{\text{T}} > 90$ GeV
	at least one b-tagged jet with $p_{\text{T}} > 40$ GeV	

6.1   The DY+jets control region

The main difference between the CR for the DY+jets background and the SR of this analysis lies in the requirement imposed on the $M_{\tau\tau}$ variable: the CR consists of the events that are vetoed in the SR selection, i.e. those events with $M_{\tau\tau}$ in the range 0-160 GeV. To further increase the efficiency for leptons from τ decays, the impact parameter variable cuts are relaxed to $IP_{3D} < 0.0175$ cm and $SIP_{3D} < 2.5$. Finally, also the upper bound of 30 GeV on the lepton p_T is removed. The region with lepton $p_T < 20$ GeV and $IP_{3D} < 0.01$ cm and $SIP_{3D} < 2$ is also removed to reduce the presence of potential signal. The trigger, lepton identification and b tagging efficiencies are corrected in the simulation via the application of scale factors measured in dedicated data control samples. The shapes of the distributions of the variables used to bin the signal regions, $M(\ell\ell)$ and the leading lepton p_T are well described. The event yields estimated from simulation and the observed event yields are listed in Table 3. The residual physics processes other than DY+jets production are subtracted from the data using the simulation before the data-to-simulation ratio is evaluated for the estimate.

Table 3: Data and simulation yields for the DY and $t\bar{t}$ control regions corresponding to a integrated luminosity of 35.9 fb^{-1} (high E_T^{miss} region) and 33.2 fb^{-1} (low E_T^{miss} region). Uncertainties are statistical.

	DY+jets CR		$t\bar{t}$ CR	
E_T^{miss}	125-200 GeV	> 200 GeV	125-200 GeV	> 200 GeV
DY+jets or $t\bar{t}$	70.1 ± 5.1	64.5 ± 3.3	1053.7 ± 9.4	535.7 ± 7.1
All SM processes	82.6 ± 5.5	75.2 ± 3.6	1170.3 ± 11.2	710.2 ± 10.6
Data	84	75	1157	680
SR scale factor	1.02 ± 0.13	0.99 ± 0.13	0.99 ± 0.03	0.94 ± 0.04

6.2   The $t\bar{t}$ (2l) control region

To obtain a sample enriched in $t\bar{t}$ events, one or two jets are required to be identified as originating from b quarks (b-tagged). To reduce potential signal contamination, the leading b-tagged jet is required to satisfy $p_T > 40$ GeV. To increase the number of events in the CR, while still avoiding potentially large signal contamination, the upper bound on the lepton p_T is also removed. The trigger, lepton identification and b tagging efficiencies are corrected in the simulation via the application of scale factors measured in dedicated data control samples. The event yields estimated from simulation and the observed event yields are shown in Table 3. The residual processes from standard model not classified as $t\bar{t}$ background are subtracted from data before the data to simulation ratio is evaluated for the $t\bar{t}$ prediction in the signal regions.

6.3   Non-prompt background

The background from non-prompt leptons, sometimes referred to as "fake" background, is evaluated using a "tight-to-loose" method. Events where at least one lepton fails the tight identification and isolation criteria but passes a looser selection ("application region") are weighted by a transfer factor based on the probabilities that non-prompt and prompt leptons, passing the loose requirements, also satisfy the tight ones.

The probability for non-prompt leptons ("fake-rate") is measured as a function of the lepton p_T and η using a data sample enriched in QCD multijet events ("measurement region"). The method has been used in several multilepton searches in CMS and is described in more detail in [47]. The measurement region is defined by the presence of exactly one loose lepton, obtained

by relaxing the isolation and impact parameter requirements, and a jet with $p_{\mathrm{T}} > 30\,\mathrm{GeV}$, separated from the lepton by $\Delta R > 0.7$. For muons, events are selected by prescaled single-lepton triggers with no isolation requirements. For electrons, a mixture of prescaled jet triggers is used. An important challenge comes from the existence of prompt leptons in the the measurement region, mostly due to W and Z production in association with jets. This electroweak contamination is subtracted using three alternative procedures that yield consistent results.

The probability for prompt leptons is taken from simulation and corrected with a data-to-simulation scale factor extracted from $Z \to \ell\ell$ events.

The fake-rate measured in QCD events has to be applied to a sample dominated by W + jets and $t\bar{t}$ events. The latter can have a different composition in terms of flavour of the jets that give rise to the non-prompt leptons, along with other kinematic differences that potentially affect the fake-rate. These effects are studied first of all by comparing the fake-rate in the simulation of these processes; consistent results across the phase space probed by this analysis are found. A closure test is then performed by applying the fake-rate measured in the QCD simulated sample to a sample of W + jets events. The yield of events passing the tight identification criteria is compared with the prediction obtained by applying the fake-rate in the application region. The method closes at a level of 40% or better; this value is used as a systematic uncertainty on the reducible background prediction when performing the signal extraction.

Moreover, in order to better constraint the contribution of the non-prompt background in the SR, a dedicated CR consisting of same-sign leptons is defined. Requiring the two lepton candidates to have the same charge increases significantly the probability that at least one of the two is a fake lepton. The region is defined using the $\widetilde{t}$ selection in the $E_{\mathrm{T}}^{\mathrm{miss}} > 200\,\mathrm{GeV}$ region, where the opposite-sign requirement of the two leptons is modified to a same-sign one. As shown in Figure 2, a fair agreement, within the uncertainties, is observed between the data and the data-driven prediction of the background from fakes. Also visible in Fig. 2, is the near absence of a signal from real leptons. The distribution of the leading lepton transverse momentum is used as input to the final fit that performs the signal extraction, as its constraining power is expected to be significant compared to the uncertainty on the measured fake rate.

7 Systematic uncertainty on the background prediction

The systematic uncertainties on the background predictions are summarized in this Section and reported relative to: (a) the corresponding specific background yield and (b) their overall effect on the final results, summarized in Table 4.

The statistical uncertainty from data yields in control and application regions is dominated by the small number of events in the "tight-to-loose" application region. It typically dominates over the other uncertainties of the prediction, especiallly for signal regions with small event yields. The effect on the corresponding background ranges from 10% to 50%, depending on the amount of yields in the predicted region. Another source of statistical uncertainty is the data and simulation statistics in the DY+jets and $t\bar{t}$ CR. The effect on the predicted yields in the SR, obtained using the ratio described in Section 6 is of the order of 13% for DY+jets and 3% for $t\bar{t}$.

Specifically for the $t\bar{t}$ background, a set of systematics uncertainties, mainly affecting the modelling of the shapes in the simulation of this physics process, have been computed. The spin correlation of the top quarks has been varied by 20%, following the measurement of CMS and ATLAS [48, 49] and also from the comparison with different generators (MADGRAPH versus
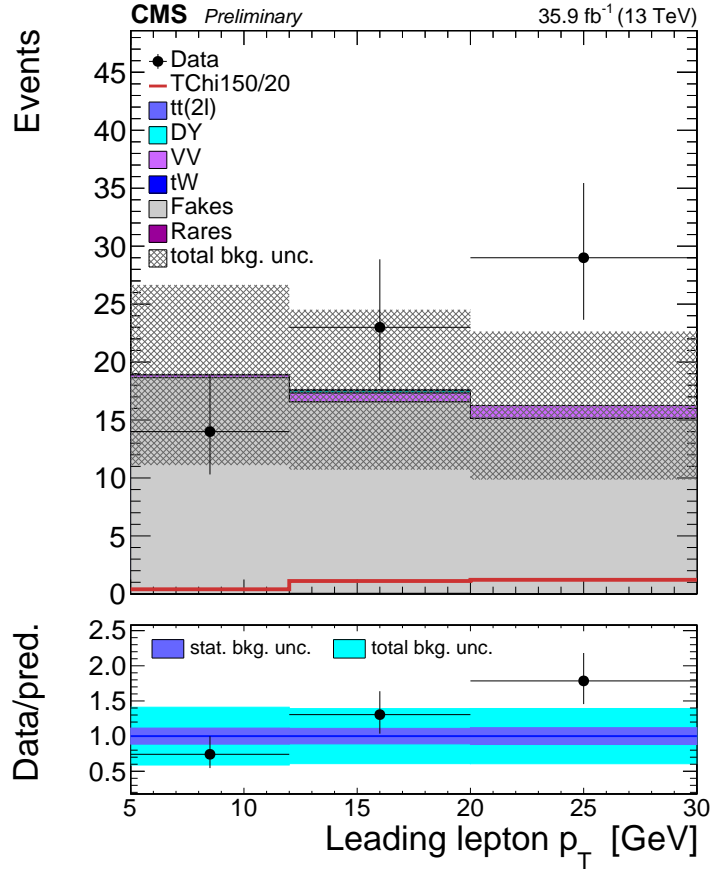
Figure 2: Same-sign control region for $\widetilde{t}$ selection and $E_T^{\text{miss}} > 200\,\text{GeV}$. The shape of of the leading lepton pT is used as input to the final signal extraction. The superimposed signal is from $\widetilde{t}$ pair production where the mass of the $\widetilde{t}$ is 350 GeV and the difference in mass with the lightest neutralino is 20 GeV (T2tt350/20).

POWHEG). Helicity amplitudes of the W boson from the top quarks decay have been varied by 5%. A top p_T modelling uncertainty has also been derived by reweighting the $t\bar{t}$ MADGRAPH events based on the number of ISR jets (N_J^{ISR}), so as to make the jet multiplicity agree with data. The reweighting factors vary between 0.92 and 0.51 for N_J^{ISR} between 1 and 6. We take one half of the deviation from unity as the systematic uncertainty on these reweighting factors. The combined effect of this set of $t\bar{t}$ modelling uncertainties on the total number of predicted $t\bar{t}$ background events ranges from 3-5%.

For the DY+jets background, the uncertainty on the recoil resolution is derived from data with $Z \to \mu\mu$ events. The uncertainty affects the DY estimation, which takes the $M_{\tau\tau}$ cut efficiency from simulation. The effect on the DY+jets predicted yields is found to be negligible ($< 1\%$).

As discussed in Section 6, the method used to estimate the non-prompt background leads to a 40% uncertainty on its normalization.

We assign 50% uncertainty to the diboson background normalization, which is checked in a dedicated region described in Section 6. In such a region, enriched in the WW process and chosen to cover a similar phase-space as the one of this search, an agreement with data, within the given uncertainty, has been observed. A conservative 100% uncertainty is assigned to the rare backgrounds (dominated by tW process).

The experimental uncertainties belonging to b tagging, trigger, leptons reconstruction, identi-

fication and isolation have been propagated and their effect on the final results ranges from 2% up to 12%. The knowledge of the jet energy scale corrections (JEC), applied to match jet energies measured in data and simulation, is affected by an intrinsic uncertainty. This affects all simulated background, leading up to typically 2-12% uncertainty on the final predictions.

An uncertainty of 2.6% is assigned to the integrated luminosity measured by the CMS experiment for the 2016 data-taking period, which affects the prediction of rare SM backgrounds relying on the measured data luminosity.

Finally, the uncertainty related to the pileup has been estimated by varying the minimumbias cross section by $\pm 5\%$ and reweighting the pileup distribution accordingly. The systematic uncertainty is of the order of 1-5%.

Table 4: Relative uncertainties on the final predictions for each individual systematic uncertainty source.

Systematic uncertainty source	typical uncertainty
Non-prompt background normalization	4-20%
DY+ jets background normalization	4-20%
$t\bar{t}$ background normalization	2-8%
$t\bar{t}$ modeling	$\lesssim 1\%$
VV background normalization	3-25%
Rare background normalization	1-3 %
Jet energy scale	2-12 %
b tagging	2-6 %
Lepton selection	1-4 %
Trigger	1-2 %

8 Results

The predicted yields of the SM background processes in the SR, and the data observed, are shown in Figures 3 and 4. The predictions in the various SR bins are extracted from a likelihood fit of data and simulation yields in the regions described in Section 6, namely the DY+jets, $t\bar{t}$ and same-sign CR. Log-normal nuisance parameters are used to describe the systematic uncertainties of Section 7 in the fit procedure. In this regard, the uncertainties on the predicted yields quoted in the following are those determined as a result of this fit.

The predicted yields along with the data are also summarized in Table 5 and Table 6 for each bin of the search region. The total uncertainty on the yield for each SM process is accounting for the systematic and statistical uncertainties described in Section 7.

9 Interpretation

The results are interpreted in terms of the simplified models for $\widetilde{\chi}_2^0\widetilde{\chi}_1^\pm \rightarrow \widetilde{\chi}_1^0\widetilde{\chi}_1^0 Z^* W^*$ and compressed $\widetilde{t} \rightarrow \widetilde{\chi}_1^\pm b$ with the subsequent decay $\widetilde{\chi}_1^\pm \rightarrow \widetilde{\chi}_1^0 W^*$ that are described in detail in Section 3. For the interpretation, a binned likelihood fit of the signal and the background expectations is performed. This fit takes as input the yields in the search regions (12 for the EWKinos interpretation and 9 for the stop interpretation) together with those in the two $t\bar{t}$ ($125 < E_T^{\mathrm{miss}} < 200$ GeV and $E_T^{\mathrm{miss}} > 200$ GeV) control regions, the two DY+jets ($125 < E_T^{\mathrm{miss}} < 200$ GeV
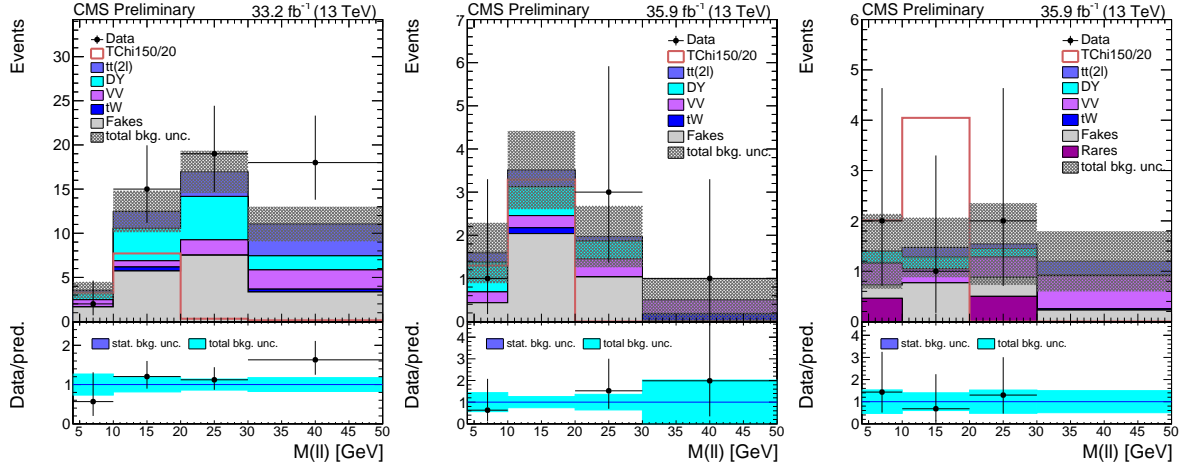
Figure 3: Left: Electroweakino search region for $125 < E_T^{miss} < 200$ GeV (muon only channel) for 33.2 fb^{-1}; Middle: $200 < E_T^{miss} < 250$ GeV (muon and electron channel) for 35.9 fb^{-1}; Right: $E_T^{miss} > 250$ GeV (muon and electron channel) for 35.9 fb^{-1}. The superimposed signal is from neutralino-chargino ($\tilde{\chi}_2^0$-$\tilde{\chi}_1^\pm$) pair production where the mass of the chargino is 150 GeV and the difference in mass with the lightest neutralino is 20 GeV (TChi150/20).

Figure 4: Left: $\tilde{t}$ search region for $125 < E_T^{miss} < 200$ GeV (muon only channel) for 33.2 fb^{-1}; Middle: $200 < E_T^{miss} < 300$ GeV (muon and electron channel) for 35.9 fb^{-1}; Right: $E_T^{miss} > 300$ GeV (muon and electron channel) for 35.9 fb^{-1}. The superimposed signal is from $\tilde{t}$ pair production where the mass of the $\tilde{t}$ is 350 GeV and the difference in mass with the lightest neutralino is 20 GeV (T2tt350/20).
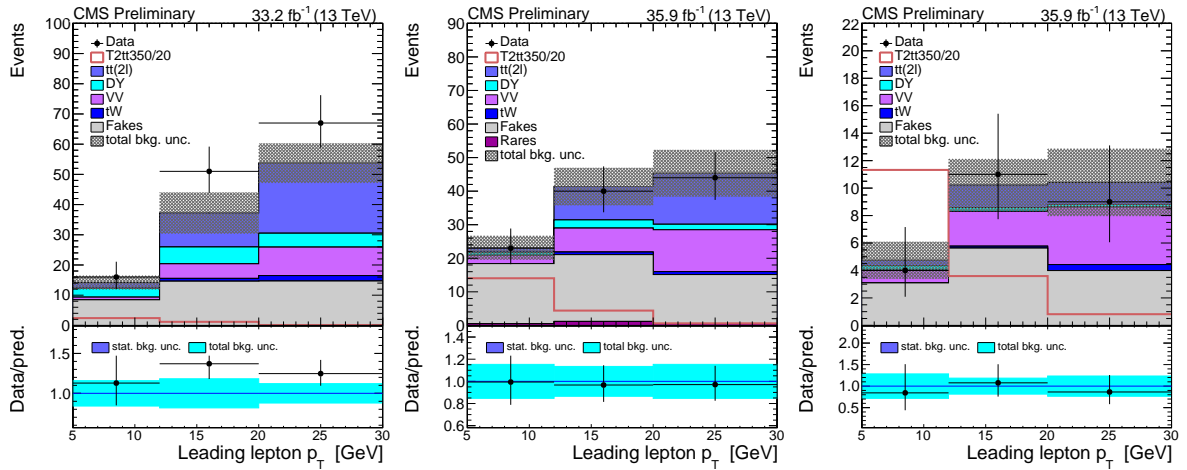
Table 5: Predicted and data yields with uncertainty from the fit for the electroweakino search region for 33.2 fb^{-1} and 35.9 fb^{-1} of integrated luminosity.

Process	$E_\mathrm{T}^\mathrm{miss}$ =[125-200] GeV			
	$4 < M_{\ell\ell} < 10$	$10 < M_{\ell\ell} < 20$	$20 < M_{\ell\ell} < 30$	$30 < M_{\ell\ell} < 50$
$t\bar{t}(2\ell)$	0.23 ± 0.16	1.9 ± 0.52	2.80 ± 0.65	3.60 ± 0.75
DY+jets	0.83 ± 0.63	3.7 ± 1.5	4.9 ± 1.5	1.60 ± 0.99
VV	0.82 ± 0.48	0.71 ± 0.65	1.7 ± 1.0	2.2 ± 1.2
Fakes	1.7 ± 0.7	5.7 ± 1.5	7.5 ± 1.7	3.3 ± 1.1
tW	–	$0.46^{+0.64}_{-0.45}$	–	$0.33^{+0.49}_{-0.32}$
Total SM Prediction	3.5 ± 1.0	12.0 ± 2.3	17.0 ± 2.4	11.0 ± 2.0
DATA	2	15	19	18

Process	$E_\mathrm{T}^\mathrm{miss}$ =[200-250] GeV			
	$4 < M_{\ell\ell} < 10$	$10 < M_{\ell\ell} < 20$	$20 < M_{\ell\ell} < 30$	$30 < M_{\ell\ell} < 50$
$t\bar{t}(2\ell)$	0.21 ± 0.17	0.38 ± 0.18	$0.11^{+0.11}_{-0.10}$	–
DY+jets	0.69 ± 0.62	0.67 ± 0.32	0.42 ± 0.27	–
VV	$0.26^{+0.28}_{-0.25}$	$0.29^{+0.32}_{-0.28}$	0.42 ± 0.33	0.33 ± 0.29
Fakes	0.44 ± 0.32	2.0 ± 0.7	1.0 ± 0.6	$0.03^{+0.14}_{-0.02}$
tW	–	$0.14^{+0.39}_{-0.13}$	–	$0.17^{+0.37}_{-0.16}$
Total SM Prediction	1.6 ± 0.7	3.5 ± 0.9	2.0 ± 0.7	$0.51^{+0.52}_{-0.50}$
DATA	1	0	3	1

Process	$E_\mathrm{T}^\mathrm{miss} > 250$ GeV			
	$4 < M_{\ell\ell} < 10$	$10 < M_{\ell\ell} < 20$	$20 < M_{\ell\ell} < 30$	$30 < M_{\ell\ell} < 50$
$t\bar{t}(2\ell)$	–	0.19 ± 0.14	0.091 ± 0.091	0.27 ± 0.14
DY+jets	0.24 ± 0.19	0.24 ± 0.17	0.17 ± 0.16	$0.014^{+0.019}_{-0.013}$
VV	0.43 ± 0.35	$0.29^{+0.29}_{-0.28}$	0.41 ± 0.29	0.66 ± 0.45
Fakes	$0.28^{+0.33}_{-0.27}$	0.77 ± 0.44	0.38 ± 0.30	0.23 ± 0.18
tW	–	–	–	$0.04^{+0.28}_{-0.03}$
Rare	$0.6^{+0.6}_{-0.5}$	–	$0.6^{+0.6}_{-0.5}$	–
Total SM Prediction	1.4 ± 0.7	1.5 ± 0.6	1.5 ± 0.8	1.2 ± 0.6
DATA	2	1	2	0

and $E_\mathrm{T}^\mathrm{miss} > 200$ GeV) control regions, and the three p_T bins of the same-sign leptons for the $E_\mathrm{T}^\mathrm{miss} > 200$ GeV control region. These background-dominated bins also help constrain further the uncertainties on the background taken from simulation and the one predicted by the "tight-to-loose" method.

As the signal yields come directly from simulation, additional systematic uncertainties are applied, which can be classified in two categories. One is the systematic uncertainty on the inclusive NLO+NLL [39, 40] cross section used for the normalization: it consists of varying the renormalization and factorization scales and the parton distribution functions. The other category is the uncertainty on the product of the signal acceptance and efficiency. The renormalization and factorization scale variation yields a total uncertainty of 3%.

Given the phase space covered by this analysis, the modeling of the ISR that leads to the boost of the produced sparticles in the transverse plane is important. For the electroweakino benchmark, the modeling of the ISR with MADGRAPH, which affects the total transverse momentum (p_TISR) of the system of hypothetical SUSY particles, is improved by reweighting the p_TISR distribution of the simulated signal events. This reweighting procedure is based on studies of the transverse momentum of Z events [26]. The reweighting factors range between 1.18 at

Table 6: Predicted and data yields with uncertainty from the fit for the $\tilde{t}$ search region for 33.2 fb^{-1} and 35.9 fb^{-1} of integrated luminosity.

Process	$E_{\mathrm{T}}^{\mathrm{miss}}$ =[125-200] GeV		
	$5 < \ell_1\,p_T < 12$	$12 < \ell_1\,p_T < 20$	$20 < \ell_1\,p_T < 30$
$t\bar{t}(2\ell)$	1.9 ± 0.4	11.0 ± 1.9	23.0 ± 3.5
DY+jets	2.9 ± 1.4	5.6 ± 1.9	4.6 ± 1.7
VV	0.8 ± 0.7	4.9 +6.3 -4.8	9.4 ± 5.4
Fakes	8.5 ± 1.9	15.0 ± 2.6	15.0 ± 2.6
tW	$0.10^{+0.16}_{-0.09}$	$0.93^{+1.0}_{-0.92}$	1.8 ± 1.7
Total SM Prediction	14.0 ± 2.3	37.0 ± 6.8	54.0 ± 6.5
DATA	16	51	67

Process	$E_{\mathrm{T}}^{\mathrm{miss}}$ =[200-300] GeV		
	$5 < \ell_1\,p_T < 12$	$12 < \ell_1\,p_T < 20$	$20 < \ell_1\,p_T < 30$
$t\bar{t}(2\ell)$	1.3 ± 0.35	9.9 ± 1.2	15 ± 2.2
DY+jets	0.92 ± 0.83	2.4 ± 0.9	1.6 ± 0.6
VV	2.5 ± 1.4	7.1 ± 4.0	12.0 ± 6.2
Fakes	18.0 ± 3.2	20.0 ± 3.4	15.0 ± 2.7
tW	–	$0.79^{+0.77}_{-0.78}$	$0.89^{+0.96}_{-0.88}$
Rare	$0.52^{+0.54}_{-0.51}$	1.2 ± 1.2	$0.57^{+0.59}_{-0.56}$
Total SM Prediction	23.0 ± 3.5	41.0 ± 5.6	45.0 ± 7.0
DATA	23	40	44

Process	$E_{\mathrm{T}}^{\mathrm{miss}} > 300$ GeV		
	$5 < \ell_1\,p_T < 12$	$12 < \ell_1\,p_T < 20$	$20 < \ell_1\,p_T < 30$
$t\bar{t}(2\ell)$	0.39 ± 0.25	1.6 ± 0.5	1.6 ± 0.4
DY+jets	0.33 ± 0.26	0.28 ± 0.18	0.19 ± 0.07
VV	0.93 ± 0.53	2.5 ± 1.4	4.2 ± 2.2
Fakes	3.1 ± 1.1	5.6 ± 1.3	4.0 ± 1.3
tW	–	$0.15^{+0.18}_{-0.14}$	$0.45^{+0.50}_{-0.44}$
Total SM Prediction	4.7 ± 1.3	10.0 ± 1.9	10.0 ± 2.5
DATA	4	11	9

p_{TISR} 125 GeV and 0.78 for $p_{\mathrm{TISR}} > 600$ GeV. The deviation from 1.0 is taken as the systematic uncertainty on the reweighting procedure. For the $\tilde{t}$ benchmark instead, in order to improve the MADGRAPH modeling of the multiplicity of additional jets from ISR, the $\tilde{t}$ signal events are reweighted based on the N_J^{ISR}, as described in Section 7. The typical uncertainties from the ISR modeling on the final results range from 2 to 7%.

We account for the different $E_{\mathrm{T}}^{\mathrm{miss}}$ reconstruction effects between full and fast simulation used for signal, and their uncertainty on the final results vary between 3 and 5%.

The uncertainties related to b tagging fast-to-full simulation factors and of the JEC corrections used to correct the signal in this search vary between 1-2%.

These uncertainties, together with those related to the predicted backgrounds described in Section 6, are added as log normal nuisance parameters in the likelihood approach.

Upper limits on the cross section of the considered benchmark models, at 95% confidence level (CL), are derived. Asymptotic results for the test statistic [50] and the CL_s criterion, as described in [51, 52] are used. Figure 5 shows the expected upper limits on the electroweakino and $\tilde{t}$ cross section values for the benchmarks considered in this search. For the electroweakino simplified model $\tilde{\chi}_2^0$ masses of up to 230 GeV for a $\Delta \mathrm{m}(\tilde{\chi}_2^0, \tilde{\chi}_1^0)$ of 20 GeV are excluded. In general,
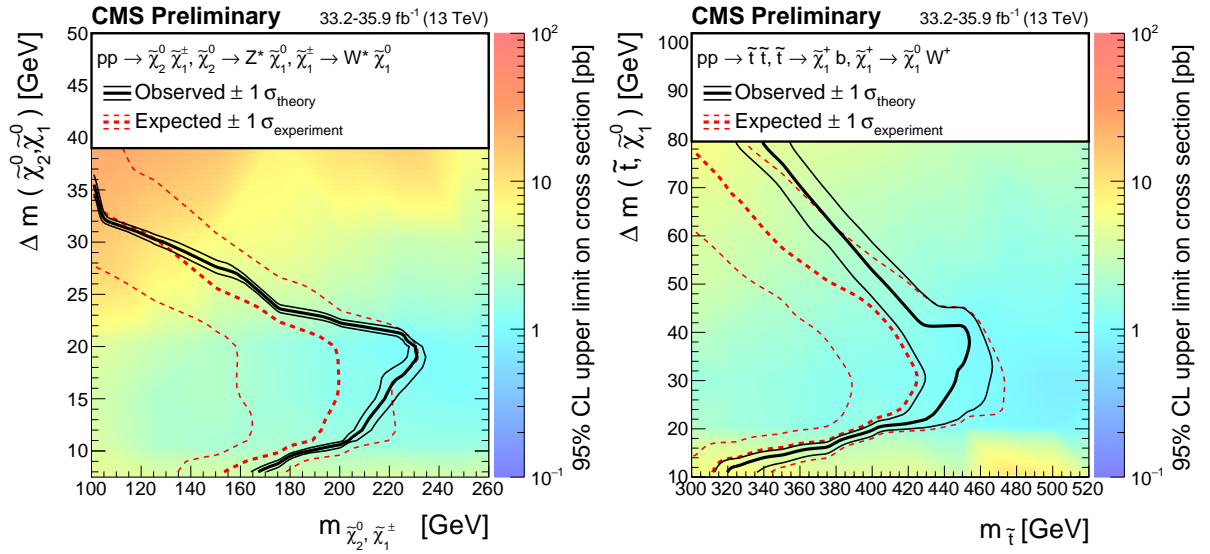
Figure 5: The observed exclusion contours (black curves) assuming the NLO+NNL cross sections, with the corresponding 1 standard deviation uncertainties for electroweakino (left) and $\tilde{t}$ (right) search. The dashed (red) curves present the expected limits with 1 standard deviation experimental uncertainties. For the electroweakino search, results are based on a simplified model of $\tilde{\chi}_2^0 \tilde{\chi}_0^\pm \rightarrow \tilde{\chi}_1^0 \tilde{\chi}_1^0 Z^* W^*$ process with a pure Wino production cross section, while a simplified model of the $\tilde{t}$ pair production, followed by the $\tilde{t} \rightarrow \tilde{\chi}_1^\pm b$ and the subsequent $\tilde{\chi}_1^\pm \rightarrow \tilde{\chi}_1^0 W^*$ decay is used for the $\tilde{t}$ search. In this last model, the mass of the $\tilde{\chi}_1^\pm$ is set to be $(M_{\tilde{t}} + M_{\tilde{\chi}_1^0})/2$. Data corresponds to an integrated luminosity ranging from 33.2 fb^{-1} to 35.9 fb^{-1}.

the observed exclusion matches with the expected one, except for the region of $\Delta m(\widetilde{\chi}_2^0, \widetilde{\chi}_1^0) = [10, 20]$ GeV where the observed curve exceeds the expected one by 1 standard deviation. This is explained by lower observed data yields with respect to predictions in the $M_{\ell\ell} = [10, 20]$ GeV range of the $200 < E_T^{\text{miss}} < 250$ GeV region, as visible in Figure 3. The existence of $\widetilde{t}$ masses up to 450 GeV with a $\Delta m(\widetilde{t}, \widetilde{\chi}_1^0)$ of 40 GeV has been ruled out for the specific model considered.

10 Summary

A search for new physics in events with two low momentum opposite-sign leptons and missing transverse energy is presented using the data collected by CMS at a a center-of-mass energy of 13 TeV and corresponding to an integrated luminosity of up to 35.9 fb^{-1}. The data are found to be consistent with the standard model expectations. The results are interpreted in the framework of supersymmetric simplified models targeting electroweakino mass-degenerate spectra and $\widetilde{t}$-$\widetilde{\chi}_1^0$ mass-degenerate benchmark scenarios. The search probes the $\widetilde{\chi}_2^0 \widetilde{\chi}_1^\pm \rightarrow \widetilde{\chi}_1^0 \widetilde{\chi}_1^0 Z^* W^*$ process for mass differences (Δm) between $\widetilde{\chi}_2^0$ and $\widetilde{\chi}_1^0$ of less than 20 GeV. Assuming Wino production cross sections, $\widetilde{\chi}_2^0$ masses up to 230 GeV are excluded for Δm of 20 GeV. For the $\widetilde{t}$ chargino-mediated decay into $\widetilde{\chi}_1^0 W^*$, $\widetilde{t}$ masses of up to 450 GeV are excluded for a $\Delta m(\widetilde{t}, \widetilde{\chi}_1^0) = 40$ GeV assuming a simplified description of the model.

References

[1] J. Wess and B. Zumino, "Supergauge transformations in four dimensions", *Nucl. Phys. B* **70** (1974) 39, `doi:10.1016/0550-3213(74)90355-1`.

[2] H. P. Nilles, "Supersymmetry, supergravity and particle physics", *Phys. Reports* **110** (1984) 1, `doi:10.1016/0370-1573(84)90008-5`.

[3] H. E. Haber and G. L. Kane, "The search for supersymmetry: Probing physics beyond the standard model", *Phys. Reports* **117** (1985) 75, `doi:10.1016/0370-1573(85)90051-1`.

[4] R. Barbieri, S. Ferrara, and C. A. Savoy, "Gauge models with spontaneously broken local supersymmetry", *Phys. Lett. B* **119** (1982) 343, `doi:10.1016/0370-2693(82)90685-2`.

[5] S. Dawson, E. Eichten, and C. Quigg, "Search for supersymmetric particles in hadron-hadron collisions", *Phys. Rev. D* **31** (1985) 1581, `doi:10.1103/PhysRevD.31.1581`.

[6] E. Witten, "Dynamical breaking of supersymmetry", *Nucl. Phys. B* **188** (1981) 513, `doi:10.1016/0550-3213(81)90006-7`.

[7] S. Dimopoulos and H. Georgi, "Softly broken supersymmetry and SU(5)", *Nucl. Phys. B* **193** (1981) 150, `doi:10.1016/0550-3213(81)90522-8`.

[8] G. R. Farrar and P. Fayet, "Phenomenology of the production, decay, and detection of new hadronic states associated with supersymmetry", *Phys. Lett. B* **76** (1978) 575, `doi:10.1016/0370-2693(78)90858-4`.

[9] R. Barbieri and G. Giudice, "Upper bounds on supersymmetric particle masses", *Nucl. Phys. B* **306** (1988) 63, `doi:10.1016/0550-3213(88)90171-X`.

[10] B. de Carlos and J. Casas, "One-loop analysis of the electroweak breaking in supersymmetric models and the fine-tuning problem", *Phys. Lett. B* **309** (1993) 320, `doi:10.1016/0370-2693(93)90940-J`, `arXiv:hep-ph/9303291`.

[11] M. Dine, W. Fischler, and M. Srednicki, "Supersymmetric technicolor", *Nucl. Phys. B* **189** (1981) 575, `doi:10.1016/0550-3213(81)90582-4`.

[12] S. Dimopoulos and S. Raby, "Supercolor", *Nucl. Phys. B* **192** (1981) 353, `doi:10.1016/0550-3213(81)90430-2`.

[13] N. Sakai, "Naturalness in supersymmetric GUTS", *Z. Phys. C* **11** (1981) 153, `doi:10.1007/BF01573998`.

[14] R. K. Kaul and P. Majumdar, "Cancellation of quadratically divergent mass corrections in globally supersymmetric spontaneously broken gauge theories", *Nucl. Phys. B* **199** (1982) 36, `doi:10.1016/0550-3213(82)90565-X`.

[15] H. Baer, A. Mustafayev, and X. Tata, "Monojet plus soft dilepton signal from light higgsino pair production at LHC14", *Phys. Rev. D* **90** (2014) 115007, `doi:10.1103/PhysRevD.90.115007`, `arXiv:1409.7058`.

[16] G. F. Giudice, T. Han, K. Wang, and L.-T. Wang, "Nearly degenerate gauginos and dark matter at the LHC", *Phys. Rev. C* **81** (2010) 115011, `doi:10.1103/PhysRevD.81.115011`, `arXiv:1004.4902`.

[17] Z. Han, G. D. Kribs, A. Martin, and A. Menon, "Hunting quasidegenerate Higgsinos", *Phys. Rev. D* **89** (2014) 075007, `doi:10.1103/PhysRevD.89.075007`, `arXiv:1401.1235`.

[18] ALEPH Collaboration, "Search for charginos nearly mass degenerate with the lightest neutralino in e+ e- collisions at center-of-mass energies up to 209-GeV", *Phys. Lett.* **B533** (2002) 223–236, `doi:10.1016/S0370-2693(02)01584-8`, `arXiv:hep-ex/0203020`.

[19] DELPHI Collaboration, "Searches for supersymmetric particles in e+ e- collisions up to 208-GeV and interpretation of the results within the MSSM", *Eur. Phys. J.* **C31** (2003) 421–479, `doi:10.1140/epjc/s2003-01355-5`, `arXiv:hep-ex/0311019`.

[20] P. Schwaller and J. Zurita, "Compressed electroweakino spectra at the LHC", *JHEP* **03** (2014) 060, `doi:10.1007/JHEP03(2014)060`, `arXiv:1312.7350`.

[21] R. Gröber, M. M. Mühlleitner, E. Popenda, and A. Wlotzka, "Light Stop Decays: Implications for LHC Searches", *Eur. Phys. J. C* **75** (2015) 420, `doi:10.1140/epjc/s10052-015-3626-z`, `arXiv:1408.4662`.

[22] C. Balázs, M. Carena, and C. E. M. Wagner, "Dark matter, light stops and electroweak baryogenesis", *Phys. Rev. D* **70** (2004) 015007, `doi:10.1103/PhysRevD.70.015007`, `arXiv:hep-ph/0403224`.

[23] CMS Collaboration, "Searches for third-generation squark production in fully hadronic final states in proton-proton collisions at $\sqrt{s} = 8$ TeV", *JHEP* **06** (2015) 116, `doi:10.1007/JHEP06(2015)116`, `arXiv:1503.08037`.

[24] ATLAS Collaboration, "Search for top squark pair production in final states with one isolated lepton, jets, and missing transverse momentum in $\sqrt{s} = 8$ TeV pp collisions with the ATLAS detector", *JHEP* **11** (2014) 118, `doi:10.1007/JHEP11(2014)118`, `arXiv:1407.0583`.

[25] ATLAS Collaboration, "Search for pair-produced third-generation squarks decaying via charm quarks or in compressed supersymmetric scenarios in pp collisions at $\sqrt{s} = 8$ TeV with the ATLAS detector", *Phys. Rev. D* **90** (2014) 052008, `doi:10.1103/PhysRevD.90.052008`, `arXiv:1407.0608`.

[26] CMS Collaboration, "Search for supersymmetry in events with soft leptons, low jet multiplicity, and missing transverse energy in protonproton collisions at $\sqrt{s}$=8 TeV", *Phys. Lett.* **B759** (2016) `doi:10.1016/j.physletb.2016.05.033`, `arXiv:1512.08002`.

[27] CMS Collaboration, "The CMS Experiment at the CERN LHC", *JINST* **3** (2008) S08004, `doi:10.1088/1748-0221/3/08/S08004`.

[28] J. Alwall et al., "MadGraph5: going beyond", *JHEP* **06** (2011) 128, `doi:10.1007/JHEP06(2011)128`, `arXiv:1106.0522`.

[29] NNPDF Collaboration, "Parton distributions for the LHC Run II", *JHEP* **04** (2015) 040, `doi:10.1007/JHEP04(2015)040`, `arXiv:1410.8849`.

[30] J. Alwall et al., "The automated computation of tree-level and next-to-leading order differential cross sections, and their matching to parton shower simulations", *JHEP* **07** (2014) 079, `doi:10.1007/JHEP07(2014)079`, `arXiv:1405.0301`.

[31] P. Nason, "A new method for combining NLO QCD with shower Monte Carlo algorithms", *JHEP* **11** (2004) 040, `doi:10.1088/1126-6708/2004/11/040`, `arXiv:hep-ph/0409146`.

[32] S. Frixione, P. Nason, and C. Oleari, "Matching NLO QCD computations with parton shower simulations: the POWHEG method", *JHEP* **11** (2007) 070, `doi:10.1088/1126-6708/2007/11/070`, `arXiv:0709.2092`.

[33] S. Alioli, P. Nason, C. Oleari, and E. Re, "A general framework for implementing NLO calculations in shower Monte Carlo programs: the POWHEG BOX", *JHEP* **06** (2010) 043, `doi:10.1007/JHEP06(2010)043`, `arXiv:1002.2581`.

[34] S. Alioli, P. Nason, C. Oleari, and E. Re, "NLO single-top production matched with shower in POWHEG: *s*- and *t*-channel contributions", *JHEP* **09** (2009) 111, `doi:10.1007/JHEP02(2010)011`, `10.1088/1126-6708/2009/09/111`, `arXiv:0907.4076`. [Erratum: JHEP **02** (2010) 011].

[35] E. Re, "Single-top Wt-channel production matched with parton showers using the POWHEG method", *Eur. Phys. J. C* **71** (2011) 1547, `doi:10.1140/epjc/s10052-011-1547-z`, `arXiv:1009.2450`.

[36] T. Sjöstrand et al., "An Introduction to PYTHIA 8.2", *Comput. Phys. Commun.* **191** (2015) 159, `doi:10.1016/j.cpc.2015.01.024`, `arXiv:1410.3012`.

[37] S. Agostinelli et al., "GEANT4 — a simulation toolkit", *Nucl. Instr. and Meth. A* **506** (2003) 250, `doi:10.1016/S0168-9002(03)01368-8`.

[38] CMS Collaboration, "The Fast Simulation of the CMS Detector at LHC", Technical Report 3, CERN, 2011.

[39] B. Fuks, M. Klasen, D. R. Lamprea, and M. Rothering, "Gaugino production in proton-proton collisions at a center-of-mass energy of 8 TeV", *JHEP* **10** (2012) 081, `doi:10.1007/JHEP10(2012)081`, `arXiv:1207.2159`.

[40] B. Fuks, M. Klasen, D. R. Lamprea, and M. Rothering, "Precision predictions for electroweak superpartner production at hadron colliders with RESUMMINO", *Eur. Phys. J. C* **73** (2013) 2480, `doi:10.1140/epjc/s10052-013-2480-0`, `arXiv:1304.0790`.

[41] CMS Collaboration, "Particle–Flow Event Reconstruction in CMS and Performance for Jets, Taus, and E_T^{miss}", CMS Physics Analysis Summary CMS-PAS-PFT-09-001, 2009.

[42] E. Chabanat and N. Estre, "Deterministic Annealing for Vertex Finding at CMS",.

[43] CMS Collaboration, "Performance of CMS muon reconstruction in pp collision events at $\sqrt{s} = 7$ TeV", *JINST* **7** (2012) P10002, `doi:10.1088/1748-0221/7/10/P10002`, `arXiv:1206.4071`.

[44] CMS Collaboration, "Studies of Higgs boson production in the four-lepton final state at $\sqrt{s} = 13$ TeV", CMS Physics Analysis Summary CMS-PAS-HIG-15-004, 2016.

[45] M. Cacciari, G. P. Salam, and G. Soyez, "The anti-k_t jet clustering algorithm", *JHEP* **04** (2008) 063, `doi:10.1088/1126-6708/2008/04/063`, `arXiv:0802.1189`.

[46] CMS Collaboration, "Identification of b quark jets at the CMS Experiment in the LHC Run 2", Technical Report CMS-PAS-BTV-15-001, 2016.

[47] CMS Collaboration, "Search for new physics with same-sign isolated dilepton events with jets and missing transverse energy at the LHC", *JHEP* **06** (2011) 077, `doi:10.1007/JHEP06(2011)077`, `arXiv:1104.3168`.

[48] ATLAS Collaboration, "Measurement of spin correlation in top-antitop quark events and search for top squark pair production in pp collisions at $\sqrt{s} = 8$ TeV using the ATLAS detector", *Phys. Rev. Lett.* **114** (2015) 142001, `doi:10.1103/PhysRevLett.114.142001`, `arXiv:1412.4742`.

[49] CMS Collaboration, "Measurements of t t-bar spin correlations and top quark polarization using dilepton final states in pp collisions at $\sqrt{s} = 8$ TeV", *Phys. Rev. D* **93** (2016), no. 5, 052007, `doi:10.1103/PhysRevD.93.052007`, `arXiv:1601.01107`.

[50] G. Cowan, K. Cranmer, E. Gross, and O. Vitells, "Asymptotic formulae for likelihood-based tests of new physics", *Eur. Phys. J. C* **71** (2011) 1554, `doi:10.1140/epjc/s10052-011-1554-0`, `10.1140/epjc/s10052-013-2501-z`, `arXiv:1007.1727`. [Erratum: Eur. Phys. J.C73,2501(2013)].

[51] T. Junk, "Confidence level computation for combining searches with small statistics", *Nucl. Instr. and Meth. A* **434** (1999) 435, `doi:10.1016/S0168-9002(99)00498-2`, `arXiv:hep-ex/9902006`.

[52] A. L. Read, "Presentation of search results: the CL_s technique", *J. Phys. G* **28** (2002) 2693, `doi:10.1088/0954-3899/28/10/313`.